

Pfaffian and fragmented states at $\nu = \frac{5}{2}$ in quantum Hall droplets

H. Saarikoski,¹ E. Tölö,² A. Harju,² and E. Räsänen^{3,4}

¹*Kavli Institute of NanoScience, Delft University of Technology, 2628 CJ Delft, the Netherlands**

²*Helsinki Institute of Physics and Department of Engineering Physics,*

Helsinki University of Technology, P.O. Box 4100, FIN-02015 HUT, Finland

³*Institut für Theoretische Physik, Freie Universität Berlin, Arnimallee 14, D-14195 Berlin, Germany*

⁴*European Theoretical Spectroscopy Facility (ETSF)*

When a gas of electrons is confined to two dimensions, application of a strong magnetic field may lead to startling phenomena such as emergence of electron pairing, which manifests itself as appearance of the fractional quantum Hall effect with a quantized conductivity at an unusual half-integer $\nu = \frac{5}{2}$ Landau level filling. Here we show that similar electron pairing may occur in quantum dots where the gas of electrons is trapped by external electric potentials into small quantum Hall droplets. However, we also find theoretical and experimental evidence that, depending on the shape of the external potential, the paired electron state can break down, which leads to a fragmentation of charge and spin densities into incompressible domains. The fragmentation of the quantum Hall states could be an issue in the proposed experiments that aim to probe for non-abelian quasi-particle characteristics of the $\nu = \frac{5}{2}$ quantum Hall state.

PACS numbers: 73.21.La, 73.43.-f, 71.10.Pm, 85.35.Be

I. INTRODUCTION

The discovery of the quantum Hall (QH) effect at Landau level filling factor $\nu = \frac{5}{2}$ in the two-dimensional electron gas (2DEG) (Ref. 1) marked evidence for existence of an exotic state of matter, a paired quantum Hall state. Since electron-electron (e-e) interactions are repulsive this pair formation is a collective phenomenon involving residual interactions of composite particles that, in this state, are composites of an electron and two vortices. The electron pairing would be analogous to the formation of Cooper pairs in superconductors, although it would be purely a result of e-e interactions without contribution from phonons or other fields. In some theoretical models, the excitations of the paired electron state are predicted to have non-abelian statistics that could be employed in the field of topological quantum computing.² Currently, the most pressing challenge is to experimentally find evidence of the paired electron state and the particle statistics of its excitations.^{3,4,5} The proposed tests⁶ for the non-abelian properties of these excitations make use of confined geometries and multiple constrictions in the 2DEG to generate interference among tunneling paths. This leads to a natural question whether the paired electron state is stable when the 2DEG is confined into narrow trappings.

This work addresses the structure of the $\nu = \frac{5}{2}$ state when electrons in the 2DEG have been confined by external potentials into small QH droplets. They can be experimentally realized by placing semiconductor quantum-dot (QD) devices into strong magnetic fields.⁷ We show here theoretical evidence that in QH droplets the Pfaffian wave function, which describes the paired electron state, may have high overlaps with the exact many-body states at $\nu = \frac{5}{2}$. In these calculations, we assume that the half-filled Landau level is spin-polarized and use realistic e-e potentials that include screening effects from the

background charge of electrons in the the lowest Landau level and a softening due to the finite thickness of the sample. However, the half-filled second Landau level of the Pfaffian state has a relatively high angular momentum, which may lead to its instability in the QD confinement. We show that in harmonic confining potentials a compact filling of the half-filled Landau level is favored leading to the lowering of its angular momentum. The paired electron state would then break down via fragmentation of spin and charge densities into two incompressible domains, spin-compensated $\nu = 2$ at the edges and spin-polarized $\nu = 3$ at the center (see Refs. 8 and 9). This phenomenon is analogous to the proposed formation of similar structures in the 2DEG where translational symmetry has been broken by long-range disorder.¹⁰ We present the fragmented states in QDs as alternatives to the Pfaffian state and show signatures of them in electron transport experiments. Based on these results, we conjecture that the stability of the paired electron state depends crucially on the shape of the potential landscape where the electrons move in the 2DEG. This may explain, e.g., the observed fragility of the $\nu = \frac{5}{2}$ QH state in narrow quantum point contacts.¹¹

The paper is organized as follows. We introduce our theoretical model of QDs in Sec. II and the computational methods used to solve the many-body problem in Sec. III. The exact diagonalization method is used in Sec. IV to calculate the overlaps of the Pfaffian wave function with the exact many-body state. In Sec. V, we analyze the electronic structure of fragmented QH states and show that the second-lowest Landau level is spin-polarized due to the lifting of degeneracy of single-particle states near the Fermi level. In Sec. VI, we present experimental evidence for fragmentation of QH states in the $2 \leq \nu \leq \frac{5}{2}$ filling-factor regime. Section VII concludes our work with discussion of the relevance of our findings with the observed fragility of the $\nu = \frac{5}{2}$ QH state in disordered or

confined 2DEG.

II. MODEL

QDs formed in the GaAs/Al_xGa_{1-x}As heterostructure are modeled for both lateral and vertical QD devices as droplets of electrons in a strictly two-dimensional (2D) plane confined by a parabolic external potential.⁷ We use an effective-mass Hamiltonian

$$H = \sum_{i=1}^N \left[\frac{(\mathbf{p}_i + e\mathbf{A})^2}{2m^*} + V_c(r_i) \right] + \frac{e^2}{4\pi\epsilon} \sum_{i<j} \frac{1}{r_{ij}}, \quad (1)$$

where N is the number of electrons, $V_c(r) = m^*\omega_0^2 r^2/2$ is the external parabolic confinement, $m^* = 0.067m_e$ is the effective mass and $\epsilon = 12.7\epsilon_0$ is the dielectric constant of the GaAs semiconductor medium, and \mathbf{A} is the vector potential of the homogeneous magnetic field \mathbf{B} perpendicular to the QD plane. The confinement strength ω_0 in the calculations is 2 meV, unless otherwise stated.

If the e-e interactions are excluded, the single-particle solutions of the Hamiltonian (1) are Fock-Darwin states.¹² In the limit of a very high magnetic field, the Landau level structure approaches that of the 2DEG. However, in finite magnetic fields the external potential alters the electronic structure and different Landau levels overlap. Therefore, the concept of Landau level filling needs to be generalized to finite-size systems. Kinaret *et al.* defined the average filling factor as $\nu_{\text{avg}} = N^2(N+L)/2$, where L is the total angular momentum.¹³ Another possibility is to focus on the lowest Landau level (LLL) and define filling factor of a state as $\nu_{\text{LLL}} = 2N/N_{\text{LLL}}$. These definitions differ in the high filling-factor regime, but this is not critical to the interpretation of results that are based on the structural properties of the many-body states.

III. COMPUTATIONAL MANY-BODY METHODS

The ground state corresponding to interacting electrons in QH droplets is solved numerically using the exact diagonalization (ED), density-functional theory (DFT), and the variational quantum Monte Carlo method (QMC). Since the paired electron state in the 2DEG is a strongly correlated many-body state, the ED method is used to analyze its stability in the QD confining potential. The DFT and QMC methods are used to analyze the fragmented QH states. The regime where this fragmentation gives characteristic signals in the experiments is beyond the reach of the ED method. However, we find that both the DFT and QMC methods provide accurate results in this regime (see Appendix).

A. Exact diagonalization

In the ED method, we assume that the electrons occupy states on one Landau level only. If we now take a fixed number of states from this Landau level, our computational task is first to construct the many-body basis. Then the Hamiltonian matrix corresponding to Hamiltonian of Eq. (1) is constructed in this basis. Finally, the lowest eigenstate and eigenvalue are found by matrix diagonalization. More details can be found, e.g., in Ref. 14. In addition to the standard Coulomb interaction, we use in the ED two modifications of it. To model the finite thickness of the sample, we use a softened potential¹⁵ defined as

$$V_T(r) = \frac{e^2}{4\pi\epsilon\sqrt{r^2 + d_T^2}}, \quad (2)$$

where d_T is the sample thickness. Electrons in second or higher Landau levels move on top of background charge of lower Landau levels, which effectively screens the Coulomb interaction. This is modeled with a screened potential that is of the Gaussian form

$$V_S(r) = \frac{e^2 \exp(-r^2/d_S^2)}{4\pi\epsilon r}, \quad (3)$$

where d_S is the screening length. The unit of length in our ED results is given by $l = \sqrt{\hbar/m^*\omega}$, where $\omega = \sqrt{\omega_0^2 + (\omega_c/2)^2}$ and $\omega_c = eB/m^*$ is the cyclotron frequency of electron in magnetic field B .

B. Density-functional theory

Our DFT approach is based on spin-DFT, a variant of the conventional DFT generalized to deal with non-zero spin polarization. On top of standard spin-DFT, we include the bare external vector potential \mathbf{A} [see Eq. (1)] in the Kohn-Sham equation. In contrast with current-spin-DFT, however, we neglect the exchange-correlation vector potential \mathbf{A}_{xc} . In the magnetic-field range considered here, this has been shown to be a very reasonable approximation.¹⁶ As another valid approximation, we neglect the dependence of the exchange and correlation on the vorticity.¹⁷ The exchange and correlation energies and potentials are calculated using the 2D local spin-density approximation, for which we use the QMC parametrization of the correlation energy by Attaccalite *et al.*¹⁸

The DFT approach is implemented on a 2D real-space grid and employs a multigrid method for solving of the Kohn-Sham equations.¹⁹ Our symmetry-unrestricted DFT approach has been shown to lead to solutions with broken rotational symmetry that has been linked to mixing of the different eigenstates of angular momentum.^{20,21} In a fixed symmetric external potential, this type of spontaneous symmetry breaking is expected to be unphysical. In Sec. VI, we compare the validity of this assumption directly to experimental data.

C. Quantum Monte Carlo

Since the fragmentation of many-body state in the vicinity of $\nu = \frac{5}{2}$ is a delicate many-body problem, we employ the QMC method to analyze the reliability of our DFT approach. The wave function in the QMC is chosen to be

$$\Psi = D_{\uparrow} D_{\downarrow} \prod_{i < j}^N J(r_{ij}), \quad (4)$$

where the two first factors are Slater determinants for the two spin types, and J is a Jastrow two-body correlation factor. The Slater determinants are constructed from the Fock-Darwin states. For the two-body Jastrow factor, we use a form

$$J(r) = \exp\left(\frac{Cr}{a + br}\right), \quad (5)$$

where a is fixed by the cusp condition to be three for a pair of equal spins and one for opposite ones, and b is an additional parameter different for both spin-pair possibilities. The ground state of the QD in the spin-droplet regime is calculated assuming that the LLL and the second-lowest Landau level (SLL) are compact. This means that the Slater determinants are built from single-particle states having angular momenta $l = 0, \dots, N_{\text{LLL},s} - 1$ for spin $s = \uparrow, \downarrow$ in the LLL and $l = -1, \dots, N_{\text{SLL},s} - 2$ for the spin s in the SLL. Energy for each combination of non-negative total spin S and total angular momentum L is then calculated. The QMC method deals with the correlation effects in the many-particle system more accurately than the DFT approach. However, the computational cost of the QMC is significantly larger than that of the DFT. A detailed description of the QMC method is given in Ref. 22.

IV. PFAFFIAN STATE IN QUANTUM DOTS

The structure of the QH states in the 2DEG at half-integer filling factor has been a topic of intense research efforts. Moore and Read predicted that the LLL of the $\nu = \frac{5}{2}$ state is spin-compensated, and the electrons in the half-filled SLL are spin-polarized and form pairs. Formally, they are described by the state with the Pfaffian wave function.²³ There exists some theoretical evidence that the excitations of this QH state obey non-abelian statistics.^{23,24} ED calculations have become standard tests of trial wave functions of QH states, and they have shown high overlaps with the Pfaffian wave function in the 2DEG.²⁵ However, there are other candidates for the $\nu = \frac{5}{2}$ state, some of which possess only abelian quasiparticle excitations.^{24,26}

The structure of the $\nu = \frac{1}{2}$ state in QDs was analyzed with the ED method in Ref. 8. Here we provide results for half-filled higher Landau levels with more realistic

inter-electron potentials defined in Sec. III. Following the theory of the $\nu = \frac{5}{2}$ QH state in the 2DEG, we assume that the half-filled Landau level is spin-polarized. The Pfaffian wave function,²³ which describes paired fermion states of the half-filled Landau level, is defined for LLL as

$$\Psi_{\text{PF}} = \text{Pf}\left(\frac{1}{z_i - z_j}\right) \prod_{i < j} (z_i - z_j)^2 \exp\left(-\frac{1}{2} \sum_i r_i^2\right). \quad (6)$$

In higher Landau levels the Pfaffian state is obtained by applying the Landau level raising operator to each electron. The angular momentum of the Pfaffian state is $L' = N'(N' - 1) - (n_{\text{LL}} + \frac{1}{2})N'$, where N' is the number of electrons in the half-filled Landau level and $n_{\text{LL}} = \{0, 1, \dots\}$ is the Landau level index.

We present the overlaps of the Pfaffian wave function with the ED eigenstate for electrons frozen to lowest (LLL), second (SLL), or third (TLL) Landau level, which correspond to filling fractions of $\nu = \frac{1}{2}$, $\nu = \frac{5}{2}$, and $\nu = \frac{9}{2}$, respectively. Electrons in the half-filled second and third Landau levels move on top of the uniform background electron density of the spin-compensated lower Landau levels. This background charge effectively screens the Coulomb interaction. In QDs, the e-e interactions are further screened due to metallic leads.

Figure 1 shows the overlaps of the Pfaffian wave function and the ED eigenstate of Coulomb interaction for particle numbers $4 \leq N' \leq 12$. For large particle numbers, the overlaps in the second Landau level are highest. This shows that $\nu = \frac{5}{2}$ has the highest probability to be described by the Pfaffian.

Next, we study how the screening of the e-e interaction and finite thickness of the sample change the overlaps of the ED eigenstate with the Pfaffian. For six electrons on LLL, the overlaps are slightly improved when the screening and finite sample thickness are taken into account in the interaction (see Fig. 2). On SLL, screening slightly improves the overlap, but a finite thickness lowers it. The same trends can be seen in Fig. 2 for eight electrons, but now the effects are clearly stronger, and there is a large increase in the overlaps. On the LLL, a finite sample thickness is needed to achieve the best overlap. On the SLL, the screening increases the overlap, which can be contrasted with the spherical geometry where the SLL overlap is maximized at a finite thickness of the sample.²⁷

The highest overlaps are of the order of 0.8–0.9 at $\nu = \frac{5}{2}$, which means that the structure of the many-body state is close to the Pfaffian. The exact state at the given angular momentum would therefore show electron pairing to a significant degree. We note that the Pfaffian wave function in Eq. (6) has no adjustable parameters. It is possible to modify the Pfaffian wave function by introducing a pairing function that differs from $g = 1/(z_i - z_j)$ of the Moore-Read form.²⁸ This won't change the angular momentum of the state but has been found to increase overlaps significantly in the 2DEG. However, the

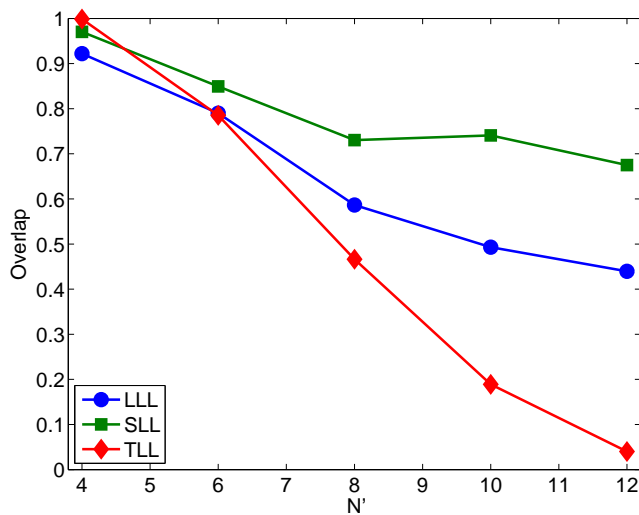


FIG. 1: (Color online) The overlaps of the Pfaffian wave function with the corresponding exact state at the lowest (LLL), second (SLL), and third (TLL) Landau level in the case of a Coulombic electron-electron interaction. N' denotes the number of electrons in the half-filled Landau level.

crucial factor that determines the stability of the paired electron states in quantum Hall droplets is whether electrons in the half-filled Landau level can attain the angular momentum of the paired electron state. In quantum Hall droplets, the degeneracy of Landau levels is lifted when electrons move in external confining potentials [Fig. 3(b)], and a compact distribution of electrons on the Landau levels could be energetically more favorable. In the next section, we show that this would lead to instability of the paired electron state and introduce fragmented QH states in quantum Hall droplets as alternatives.

V. FRAGMENTED QUANTUM HALL STATES

In quantum Hall droplets, single-particle states within each Landau level are not degenerate due to the confining potential. The average distance of an electron from the center of the droplet, and therefore also the potential energy, increase with angular momentum. This suggests that a compact occupation structure may be energetically favorable. The compact occupation of Landau levels leads to fragmentation of charge and spin densities into incompressible integer filling factor domains. We call these states fragmented quantum Hall states that are alternatives to the paired electron state at half-integer Landau level fillings.

We analyze the structure of fragmented QH states near $\nu = \frac{5}{2}$ in a harmonic confining potential of a semiconductor quantum dot with the QMC and the DFT methods. The Kohn-Sham single-particle energy spectrum of the Landau levels calculated with the spin-compensated DFT and the spin-DFT are shown in Fig. 3(a) and (b),

respectively. The spin-DFT and the QMC show that the degeneracy of the single-particle states close the Fermi energy is lifted via a complete polarization of the second-lowest Landau level. Therefore, a compact occupation of the single-particle states of the spin-compensated LLL and spin-polarized SLL leads to a fragmented state with a $\nu = 2$ region (double-occupied LLL) at the edges of the droplet and $\nu = 3$ (spin-polarized SLL) at the center [Fig. 4].

The spin-splitting of the SLL in the spin-DFT calculations is analogous to the Stoner criterion, which states that in the presence of correlations between electrons of the same spin and high density of states near the Fermi level, the system prefers ferromagnetic alignment that reduces the degeneracy.²⁹ We call the incompressible, spin-polarized droplet of SLL electrons a *spin droplet*.⁹ The size of the spin-droplet becomes significant when the number of electrons in the dot $N \gtrsim 35$. The non-uniform filling-factor structure of the spin-droplet states is reminiscent of the incompressible QH domains that form in the 2DEG with long-range disorder.¹⁰ The compact occupation of the SLL leads to a lower angular momentum than what is needed for a paired electron state as described by the Pfaffian wave function (6). For example, the size of the spin-droplet in the QMC method is $N' = 8$ electrons at $N = 48$, and the angular momentum of the SLL is $L' = 20$, which can be contrasted to $L' = 44$ for the Pfaffian wave function with the same number of electrons.

The SLL remains polarized and compact between $\frac{5}{2} \geq \nu \geq 2$. Hence, we call this filling-factor range the spin-droplet regime. The size of the spin-droplet gradually shrinks with the increasing magnetic field as the electrons are passed from the SLL to the LLL. The contributions of the LLL and SLL occupancies to the electron and spin densities are shown in Fig. 4 for the case of 60-electron QD. Qualitatively similar results were obtained for confinement strengths 1 to 4 meV and electron numbers N between 35 and 120, which confirms the generality of the results. The calculations show that the energy benefit from the polarization of the SLL is large (see Fig. 3 and Appendix), which would make spin-droplets robust in the presence of impurities in samples.

We note that the stability of the fragmented QH states in large QDs ($N > 30$) can be contrasted to the instability of the maximum-density-droplet (MDD) state in the same regime. The MDD state is the totally polarized state corresponding to the $\nu = 1$ QH state in 2DEG, and it has been found to be unstable in large QDs with $N > 30$ (Refs. 30 and 31).

VI. SIGNATURES OF FRAGMENTATION IN ELECTRON AND SPIN TRANSPORT

The emergence of finite size counterparts of integer and fractional QH states in QDs gives characteristic signatures in the chemical potentials. Several experimental

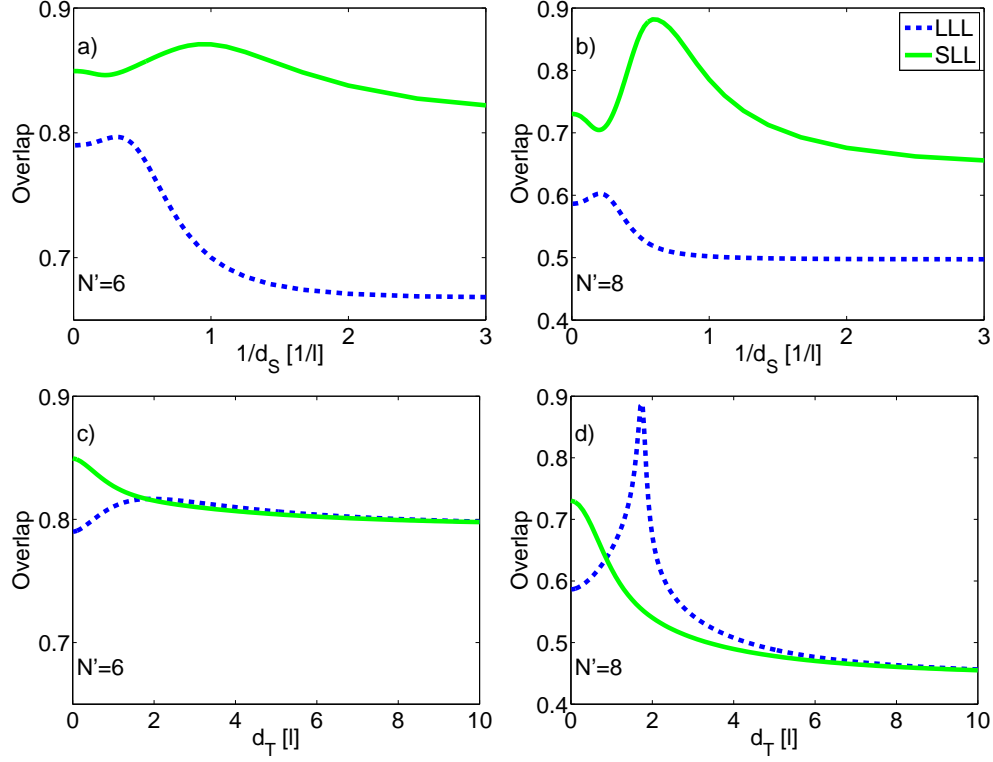


FIG. 2: Overlap of the Pfaffian wave function with the corresponding exact state for $N' = 6$ and $N' = 8$ electrons in the half-filled Landau level, respectively, using (a-b) screened electron-electron potential with screening length d_S and (c-d) softened potential due to finite sample thickness d_T for electrons at the lowest Landau level (LLL) corresponding to $\nu = \frac{1}{2}$, and the second lowest Landau level (SLL) corresponding to $\nu = \frac{5}{2}$.

methods have been developed to measure the chemical potential in a QD via addition of electrons one-by-one into the system. These experimental methods include Coulomb blockade,³² capacitance,³³ and charge detection techniques.³⁴ In this work, we use data from electron transport measurements of QDs in the Coulomb and spin blockade regime.^{31,35} The spacings of the spin and Coulomb blockade peaks correspond to the energy needed to add the N th electron in the system of $N - 1$ electrons, i.e., the chemical potential defined as $\mu(N, B) = E_{\text{tot}}(N, B) - E_{\text{tot}}(N - 1, B)$.

We calculate the signatures in the chemical potentials associated with the formation of fragmented QH states and compare these to those obtained from the electron transport data in three different QD devices. Two of the experimental samples (sample A and B) are lateral quantum dots on a high-mobility 2DEG³⁵ while the third one (sample C) is a vertical QD.³¹ The samples A and B were manufactured on a high mobility 2DEG samples with spin-polarized leads for electron transport measurements in the spin blockade regime. The data of the sample C was obtained in the Coulomb blockade. The high mobility of samples chosen for comparison is essential to reduce unpredictable effects of impurities and disorder that make identification of signals of physical phenomena difficult.

We first address the problem of whether the electronic states in the QD samples show any signs of broken rotational symmetry. Inhomogeneities and impurities in QD devices may break the rotation symmetry, and a Jahn-Teller type of mechanism could be active if disorder alters significantly the shape of the confining potential. As a result, the ground state transitions with increasing magnetic field become continuous rather than discrete. A signature of this type of symmetry breaking would be a smoothing of the chemical potential. Experimental data from a high-mobility lateral QD device is of sufficiently good quality to test for the presence of symmetry breaking mechanisms. Figure 5 shows a comparison of the electron transport data to DFT calculations with and without symmetry breaking. The data shows sharp increases in the chemical potentials, which is consistent with discrete transitions in the ground state. Therefore, to a good approximation, the rotational symmetry is preserved in high mobility samples, and the angular momentum L is a good quantum number.

The complete polarization of the SLL at $\nu = \frac{5}{2}$ is reflected in the energetics of the system. The DFT calculations show that at $\nu = \frac{5}{2}$ there is a step feature followed by a plateau region in the chemical potential. Figure 6 shows the DFT results for chemical potentials of $N = 24 \dots 48$ in comparison with the experiments.

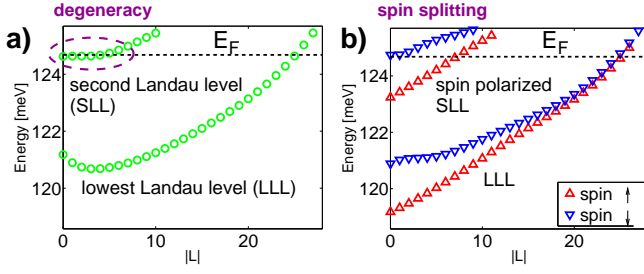


FIG. 3: (Color online) (a) Kohn-Sham energy spectrum of a 60-electron quantum dot as a function of single-particle angular momentum L calculated from the density functional theory with spin-compensated orbitals. The density of states of the second-lowest Landau level (SLL) is high near the Fermi energy E_F . The magnetic field is 2.125 T which corresponds to a filling factor of $\nu = \frac{5}{2}$. (b) The corresponding energy spectrum from spin-density functional theory shows lifting of the degeneracy near the Fermi level via complete spin polarization of the SLL. The lowest Landau level (LLL) remains spin compensated. Spin \uparrow (\downarrow) corresponds to spin orientation parallel (antiparallel) to the magnetic field. The spin-splitting due to many-body effects is about 1.5 meV at $L = 0$. In comparison, the Zeeman splitting is about 0.05 meV.

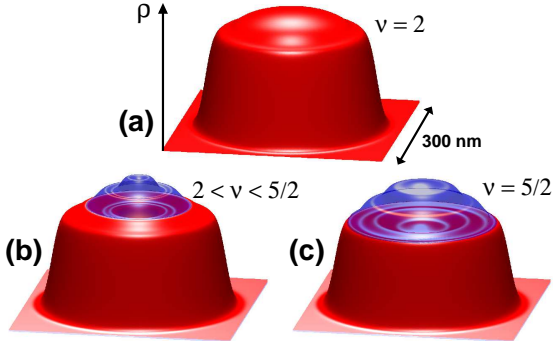


FIG. 4: (Color online) Total electron density $\rho_{\uparrow} + \rho_{\downarrow}$ (full region) and the net spin density $\rho_{\uparrow} - \rho_{\downarrow}$ (transparent blue region) of quantum Hall states in a quantum dot at (a) $\nu = 2$, at (b) an intermediate state between $\nu = 2$ and $\nu = \frac{5}{2}$, and at (c) $\nu = \frac{5}{2}$. The latter two show fragmented charge and spin densities with spin-compensated $\nu = 2$ region at the edges and spin-polarized $\nu = 3$ at the center. The densities were calculated with the spin-density-functional theory for a 60-electron quantum dot. The net spin-up density is due to spin polarization of the second-lowest Landau level.

The step in the chemical potential is associated with the total polarization of the SLL in the DFT calculations. This feature can be found in all three samples we studied above $N \geq 30$, as predicted by the theory. Some models of QDs assume that the SLL is spin-polarized due to the Zeeman effect.³⁶ This model does not, however, apply for the lateral and vertical QD devices examined in this work where the effect of the Zeeman splitting is estimated to be only a few percent of the spin splitting caused by the many-body interactions (see Fig. 3).

In the $\frac{5}{2} > \nu > 2$ regime, the ground state energy is

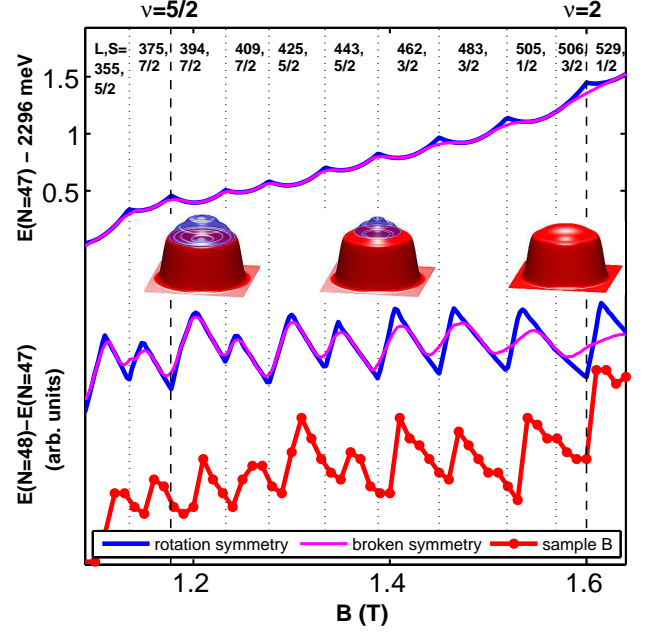


FIG. 5: (Color online) Ground state energy of the $N = 47$ quantum dot calculated with the density-functional theory for the rotationally symmetric eigenstates of the angular momentum L (blue curve) and for the ground states in the symmetry-unrestricted approach (magenta curve). The corresponding chemical potentials $\mu(N = 47 \rightarrow 48)$ calculated from the theory are shown in the lower panel together with experimental data from a lateral quantum-dot device (sample B). Dashed lines correspond to the boundaries of the spin-droplet regime. The insets show the fragmented spin and charge densities of three of the corresponding states (cf. Fig. 4). The strength of the parabolic confining potential of the quantum dot is $\omega_0 = 2$ meV in the calculations.

approximately constant (see Appendix), and the calculations show a phase transition in the system where two phases ($\nu = 2$ and $\nu = 3$) coexist, and the size of the $\nu = 2$ domain increases with the magnetic field. The chemical potential does not continue to rise, but instead, it is oscillating around a constant value until $\nu = 2$. This signature can be found in all the experimental samples (see Fig. 6). All electron transport data presented are thus consistent with the theoretical picture that the ground states in the vicinity of $\nu = \frac{5}{2}$ involve fragmented QH states. We point out, however, that the results are sensitive to the shape of the external potential, and the pairing of the electrons may still occur if the potential is sufficiently homogeneous, e.g., in large QDs, where the second Landau level would acquire higher angular momentum.

Spin polarization of the leads is commonly used to create a current that depends on the orientation of the electron spin, which passes through the device. In the case of the two lateral QDs in our analysis, the electrons enter the QD from spin-polarized magnetic edge states of the 2DEG through tunneling barriers. Coulomb block-

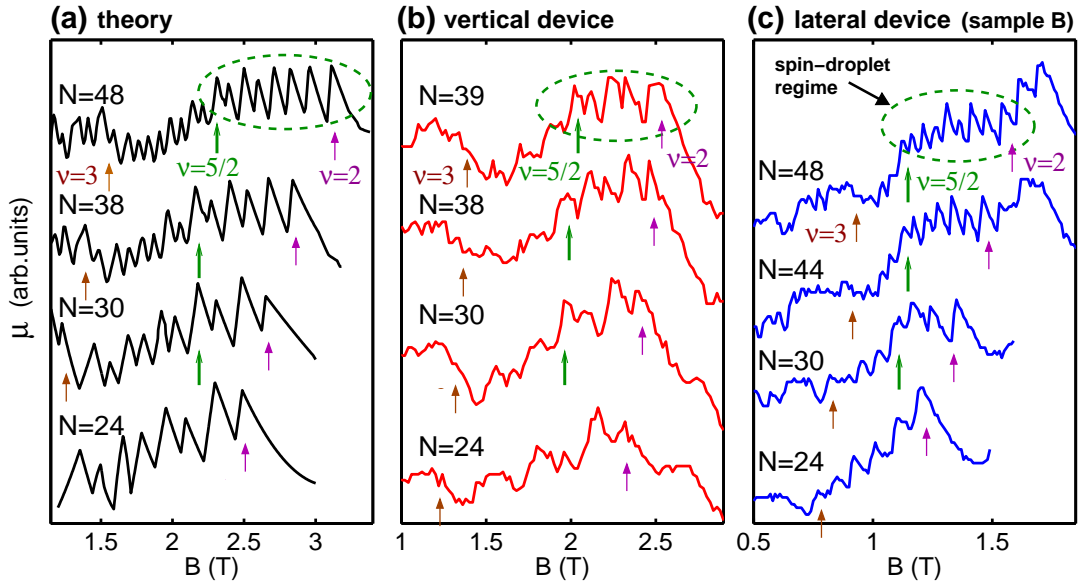


FIG. 6: (Color online) Chemical potentials calculated with the density-functional theory (a) and measured from a vertical (b) and lateral (c) quantum-dot devices for various electron numbers. Both experiments show the signal associated with the polarization of the second lowest Landau level at $\nu = 5/2$ in the peak position data when $N \gtrsim 30$ in agreement with the theoretical result. The confinement strength ranged from 2 to 4 meV depending on the electron number. The data for the vertical device in (b) is courtesy of L. Kouwenhoven³¹, and the data for lateral device in (c) is courtesy of A. S. Sachrajda.³⁵

ade lifts when the energies of the many-body states corresponding to N and $N + 1$ electrons are equal. The tunneling current depends then on the coupling between the wave function in the QD and the electronic states in the external leads. The lowest Landau level orbitals are at the edges of the QD, and the coupling is stronger to the leads compared to the second lowest Landau level orbitals that are close to the center of the QD. Due to polarization of the leads, their coupling to electron states with spin parallel to the external polarization is higher than the coupling of spins antiparallel to the external polarization. This spin dependence in the transport has been shown to lead to a characteristic checkerboard pattern of current densities through QDs.^{35,37,38,39,40} Our DFT results are consistent with such transport currents in the spin blockade regime (Fig. 7). The polarization of the SLL in the $\frac{5}{2} \geq \nu \geq 2$ regime would be in contrast to the model presented in Ref. 37. A consequence of this is that the transport current via SLL orbitals should show no checkerboard pattern in this regime since the spins are always parallel to the polarization of the leads. This could be tested with high-accuracy spin blockade spectroscopy which would be able to detect small changes in the weak tunneling currents through the SLL orbitals.

VII. FRAGILITY OF THE $\nu = \frac{5}{2}$ QUANTUM HALL STATE

The $\nu = \frac{5}{2}$ state is one of the most fragile QH states. It is observed only in high-mobility 2DEG samples as the

paired electron state may break down in the presence of impurities. These induce a non-uniform potential that, in the light of results in this work, may lead to its instability. Our findings are thus in line with those obtained by Chklovskii and Lee who predicted that in the presence of long-range disorder in the 2DEG, incompressible integer filling factor regions form that are separated by domain walls.¹⁰ These structures are analogous to the fragmented QH states that we find in QDs. Structures reminiscent of domain walls have been observed with scanning-probe imaging techniques in a perturbed QH liquid.⁴¹

Analogous instability of QH states may also occur in other geometries where the electrons are not strictly confined in all directions, such as in high-mobility 2DEG samples in the vicinity of constrictions. One indication of this may be the observed fragility of the $\nu = \frac{5}{2}$ state in narrow quantum point contacts.¹¹ Proposed tests⁶ for the non-abelian properties of quasi-particle excitations of $\nu = \frac{5}{2}$ QH state make use of finite geometries and multiple constrictions to generate interference among tunneling paths. A possible fragmentation of the $\nu = \frac{5}{2}$ QH state close to the boundaries, which would lead to the instability in such geometries, is still an open question that requires further analysis of the effects of the confinement. While recent experiments on the quasi-particle tunneling,³ shot noise generated by partitioning edge currents,⁴ and interferometric measurements of QH edge excitations⁵ of the $\nu = \frac{5}{2}$ QH state show results, which are all consistent with the unusual quasi-particle charge $e^* = \frac{1}{4}$ of the paired electron state, the particle statistics of the excitations remains to be confirmed.

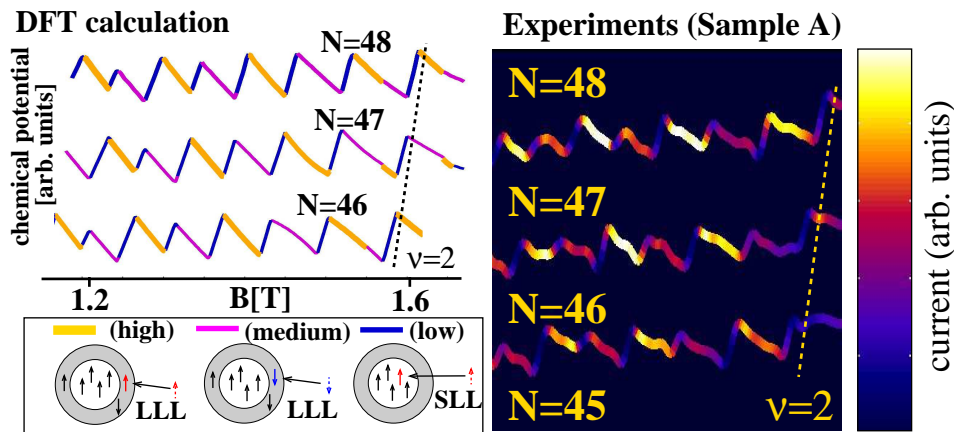


FIG. 7: (Color online) Checkerboard pattern of transport current in density-functional theory (left panel) and spin-blockade experiments (right panel). The lowest current densities correspond to electron transport via states in the second-lowest Landau level, near the core of the quantum dot. The current density in experiments has been amplified in high magnetic fields with a linear function to compensate for the general attenuation of the signal.

Possible fragmentation of QH states in narrow constrictions needed for quasi-particle interferometry adds another challenge in this long quest to confirm the possible non-abelian characteristics of the $\nu = \frac{5}{2}$ state.

To conclude, we have shown theoretical evidence that electron pairing is possible in small QH droplets in quantum dots at $\nu = \frac{5}{2}$, provided that the half-filled Landau level can acquire sufficiently high angular momentum. However, our calculations indicate that in parabolic external confining potentials the paired electron state breaks down leading to fragmentation of charge and spin densities. We find indirect evidence of such fragmentation in several experiments but point out that our results can be tested by direct measurements of the spatial dependence of spin and charge densities in different geometries and experimental setups.

Acknowledgments

We gratefully acknowledge valuable discussions with A. S. Sachrajda, M. Ciorga, S. M. Reimann, and L. Kouwenhoven, and thank Jaakko Nissinen for calculating the Pfaffian interaction matrix elements. This work was supported by the EU's Sixth Framework Programme through the Nanoquanta Network of Excellence (NMP4-CT-2004-500198), the Academy of Finland, and the Finnish Academy of Science and Letters through the Viljo, Yrjö and Kalle Väisälä Foundation.

VIII. APPENDIX: ACCURACY OF NUMERICAL METHODS

The electron correlations play an important role in the structure of fractional QH states. To test for the accuracy of the DFT method in the spin-droplet regime, we

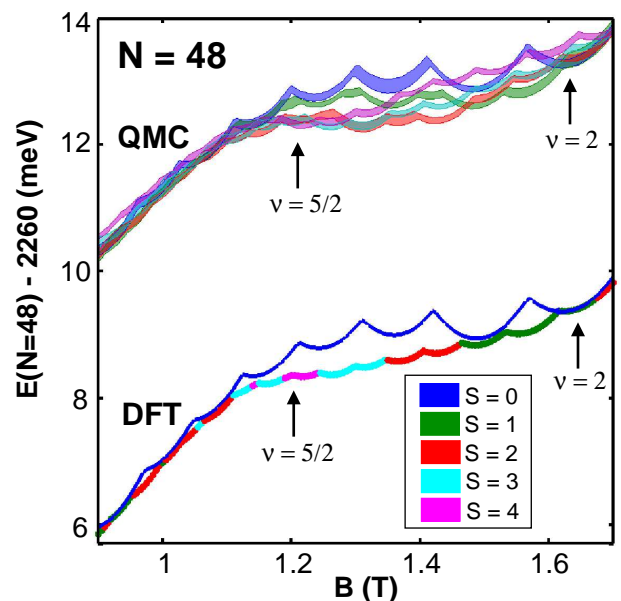


FIG. 8: (Color online) Comparison of the ground state energies for given total spin S in the density-functional theory (DFT) and the quantum Monte Carlo (QMC) method. The number of electrons $N = 48$. The line widths in the QMC denote the statistical error in the results. Only the ground state and the $S = 0$ state are shown in the DFT result. The strength of the parabolic confining potential of the quantum dot is $\omega_0 = 2$ meV in the calculations.

compare the energies of different spin polarization states between the DFT and the QMC in the $\frac{5}{2} \geq \nu \geq 2$ regime. The results for a 48-electron QD are shown in Fig. 8.

Both methods show the spin-droplet structure with a comparable energy benefit in the polarization $\delta \approx 0.5$ meV for $S_{\max} = 4$. The QMC method estimates that the maximum size of the spin droplet is $N_{SD} = 7$ compared to

8 in the DFT. Given the typical statistical error of ± 0.05 meV in the QMC results, the overall agreement between the methods is excellent. This test indicates that the DFT method captures the essential many-body physics of the spin-droplet formation and gives accurate results for the ground states. The DFT method was subsequently used in the calculation of the chemical potentials of large QDs, which can be compared to the transport experiments in the spin blockade regime.

The DFT method predicts some non-compact states

outside the spin-droplet regime, e.g., $L = 375$, $S = 7/2$ state as shown in Fig. 5. This state has one spin-down electron in the SLL with $l = 0$. Emergence of non-compact states is a manifestation of the degeneracy of the single-particle states near Fermi-level. However, they are rare in the DFT and occur only at magnetic fields below the polarization of the SLL. Detailed analysis of these states with the QMC goes beyond the scope of the present work and is left for future research.

-
- * Electronic address: h.m.saarikoski@tudelft.nl
- ¹ R. Willett, J. P. Eisenstein, H. L. Störmer, D. C. Tsui, A. C. Gossard, and J. H. English, *Phys. Rev. Lett.* **59**, 1776 (1987).
 - ² C. Nayak, S. H. Simon, A. Stern, M. Freedman, and S. D. Sarma, arXiv:0707.1889 (2007).
 - ³ I. P. Radu, J. B. Miller, C. M. Marcus, M. A. Kastner, L. N. Pfeiffer, and K. W. West, *Science* **320**, 899 (2008).
 - ⁴ M. Dolev, M. Heiblum, V. Umansky, A. Stern, and D. Mahalu, *Nature* **452** 829 (2008).
 - ⁵ R. L. Willett, M. J. Manfra, L. N. Pfeiffer, and K. W. West, arXiv:0807.0221 (2008).
 - ⁶ A. Stern and B. I. Halperin, *Phys. Rev. Lett.* **96**, 016802 (2006); P. Bonderson, A. Kitaev, and K. Shtengel, *Phys. Rev. Lett.* **96**, 016803 (2006); D. E. Feldman and A. Kitaev, *Phys. Rev. Lett.* **97**, 186803 (2006).
 - ⁷ S. M. Reimann and M. Manninen, *Rev. Mod. Phys.* **74**, 1283 (2002).
 - ⁸ A. Harju, H. Saarikoski, and E. Räsänen, *Phys. Rev. Lett.* **96**, 126805 (2006).
 - ⁹ E. Räsänen, H. Saarikoski, A. Harju, M. Ciorga, and A. S. Sachrajda, *Phys. Rev. B* **77**, 041302(R) (2008).
 - ¹⁰ D. B. Chklovskii and P. A. Lee, *Phys. Rev. B* **48**, 18060 (1993).
 - ¹¹ J. B. Miller, I. P. Radu, D. M. Zumbuhl, E. M. Levenson-Falk, M. A. Kastner, C. M. Marcus, L. N. Pfeiffer, and K. W. West, *Nat. Phys.* **3**, 561 (2007).
 - ¹² V. I. Fock, *Z. Phys.* **47**, 446 (1928); C. G. Darwin, *Proc. Cambridge Philos. Soc.* **27**, 86 (1930).
 - ¹³ J. M. Kinaret, Y. Meir, N. S. Wingreen, P. A. Lee, and X. G. Wen, *Phys. Rev. B* **46**, 4681 (1992).
 - ¹⁴ S. S. Gylfadottir, A. Harju, T. Jouttenus, and C. Webb, *New J. of Phys.* **8**, 211 (2006).
 - ¹⁵ F. C. Zhang and S. Das Sarma, *Phys. Rev. B* **33**, 2903 (1986).
 - ¹⁶ N. Helbig, S. Kurth, S. Pittalis, E. Räsänen, and E. K. U. Gross, *Phys. Rev. B* **77**, 245106 (2008).
 - ¹⁷ H. Saarikoski, E. Räsänen, S. Siljamäki, A. Harju, M. J. Puska, and R. M. Nieminen, *Phys. Rev. B* **67**, 205327 (2003).
 - ¹⁸ C. Attaccalite, S. Moroni, P. Gori-Giorgi, and G. B. Bachelet, *Phys. Rev. Lett.* **88**, 256601 (2002).
 - ¹⁹ T. Torsti, T. Eirola, J. Enkovaara, T. Hakala, P. Havu, V. Havu, T. Höynälänmaa, J. Ignatius, M. Lyly, I. Makkonen, T. Rantala, K. Ruotsalainen, E. Räsänen, H. Saarikoski, and M. J. Puska, *Phys. Stat. Sol. (b)* **243**, 1016 (2006).
 - ²⁰ K. Hirose and N. Wingreen, *Phys. Rev. B* **59**, 4604 (1999).
 - ²¹ A. Harju, E. Räsänen, H. Saarikoski, M. J. Puska, R. M. Nieminen, and K. Niemelä, *Phys. Rev. B* **69**, 153101 (2004).
 - ²² A. Harju, *J. Low Temp. Phys.* **140**, 181 (2005).
 - ²³ G. Moore and N. Read, *Nucl. Phys. B* **360**, 362 (1991).
 - ²⁴ C. Nayak and F. Wilczek, *Nucl. Phys. B* **479**, 529 (1996).
 - ²⁵ E. H. Rezayi and F. D. M. Haldane, *Phys. Rev. Lett.* **84**, 4685 (2000).
 - ²⁶ B. J. Overbosch and X. G. Wen, arXiv:0804.2087 (2008).
 - ²⁷ M. R. Peterson, Th. Jolicoeur, and S. Das Sarma, *Phys. Rev. Lett.* **101**, 016807 (2008).
 - ²⁸ G. Möller and S.H. Simon, *Phys. Rev. B* **77**, 075319 (2008).
 - ²⁹ E. C. Stoner, *Proc. Roy. Soc. A* **165**, 372 (1938).
 - ³⁰ M. Ferconi and G. Vignale, *Phys. Rev. B* **56**, 12108 (1993); O. Klein, C. de C. Chamon, D. Tang, D. M. Abusch-Magder, U. Meirav, X.-G. Wen, M. A. Kastner, and S. J. Wind, *Phys. Rev. Lett.* **74**, 785 (1999).
 - ³¹ T. H. Oosterkamp, J. W. Janssen, L. P. Kouwenhoven, D. G. Austing, T. Honda, and S. Tarucha, *Phys. Rev. Lett.* **82**, 2931 (1999).
 - ³² P. L. McEuen, E. B. Foxman, U. Meirav, M. A. Kastner, Y. Meir, N. S. Wingreen, and S. J. Wind, *Phys. Rev. Lett.* **66**, 1926 (1991).
 - ³³ R. C. Ashoori, H. L. Stormer, J. S. Weiner, L. N. Pfeiffer, S. J. Pearton, K. W. Baldwin, and K. W. West, *Phys. Rev. Lett.* **68**, 3088 (1992).
 - ³⁴ M. Field, C. G. Smith, M. Pepper, D. A. Ritchie, J. E. F. Frost, G. A. C. Jones, and D. G. Hasko, *Phys. Rev. Lett.* **70**, 1311 (1993).
 - ³⁵ M. Ciorga, A. S. Sachrajda, P. Hawrylak, C. Gould, P. Zawadzki, S. Jullian, Y. Feng, and Z. Wasilewski, *Phys. Rev. B* **61**, R16315 (2000).
 - ³⁶ O. Astafiev, V. Antonov, T. Kutsuwa, and S. Komiyama, *Phys. Rev. B* **62**, 16731 (2000).
 - ³⁷ M. Keller, U. Wilhelm, J. Schmid, J. Weis, K. v. Klitzing, and K. Eberl, *Phys. Rev. B* **64**, 033302 (2001).
 - ³⁸ K. Hitachi, M. Yamamoto, and S. Tarucha, *Phys. Rev. B* **74**, 161301(R) (2006).
 - ³⁹ D. Kupidura, M. C. Rogge, M. Reinwald, W. Wegscheider, and R. J. Haug, *Phys. Rev. Lett.* **96**, 046802 (2006).
 - ⁴⁰ M. C. Rogge, C. Fühner, and R. J. Haug, *Phys. Rev. Lett.* **97**, 176801 (2006).
 - ⁴¹ S. H. Tessmer, P. I. Glicofridis, R. C. Ashoori, L. S. Levitov, and M. R. Melloch, *Nature (London)* **392**, 51 (1998).